Microelectronics Reliability 61 (2016) 48–55

Contents lists available at ScienceDirect

Microelectronics Reliability

journal homepage: www.elsevier.com/locate/mr

Numerical study of microbump failure in 3D microelectronic structures

Y.-L. Shen *, G.C. Flores, J. Guthrie

Department of Mechanical Engineering, University of New Mexico, Albuquerque, NM 87131, USA

ARTICLE INFO

Article history:
Received 31 August 2015
Received in revised form 22 December 2015
Accepted 11 January 2016
Available online 16 January 2016

Keywords:
3D microelectronics
Finite element analysis
Microbump
Failure

ABSTRACT

Microbump failure in 3D microelectronic chip stacks is studied numerically using the finite element method. The microbump structure consists of a solder joint sandwiched between copper pads connected to through-silicon vias. The model system is subject to prescribed shear deformation, with possible superimposed tension or compression. A ductile damage model for solder is implemented to investigate failure propensity and cracking pattern as affected by the loading mode and underfill material. Failure of the solder is found to be sensitive to the loading mode, with a superimposed tension or compression on shear easily changing the crack path and tending to reduce the solder ductility.

1. Introduction

Adoption of the three-dimensional (3D) platform for a wide range of applications in microelectronics has commenced. The 3D stacking of semiconductor chips offers unique advantages including the increased device density per volume, utilization of short vertical interconnection for improved electrical performance, reduced power consumption, and the capability of integrating multiple functionalities into a single package [1–3]. The signal path between stacked silicon (Si) chips is provided by the through-silicon-vias (TSVs) along with solder microbumps, as schematically shown in Fig. 1. Larger solder balls are used for joining the chip stack and the packaging substrate. Underfill or bonding material may be applied in the gap region between chips.

Mechanical integrity of 3D microelectronic devices and packages is of critical importance. Mismatches in the coefficient of thermal expansion among different materials can lead to internal stress generation during processing and operation. Another important challenge is the accurate alignment of the individual chips, which can be exacerbated by chip warpage. Misalignment of chips inevitably subjects the microbumps to shear deformation [3–5]. One of the most difficult issues during subsequent chip bonding processes is in fact the behavior of the bonding layer between already-stacked chips [6]. More complex loading modes, such as shear with superimposed tension or compression, can also exist in the case of chip warpage or other forms of chip–package interaction [7].

The present study focuses on deformation and fracture of solder microbump under predominantly shear loading. Numerical simulations incorporating a ductile damage model are employed to study the propensity of solder failure in a representative 3D chip bonding structure. In particular, we attempt to investigate the effects of underfill material on microbump failure, and how the superimposed tension/compression on shear loading can affect the cracking pattern and fracture strain.

2. Numerical model description

The finite element model uses a representative layout to capture the basic physical features of the Si chip, copper (Cu) TSV, solder material and underfill layer (when existent). Fig. 2 shows the model geometry. The simulation domain ABCD may be viewed conceptually as a representative area segment highlighted by the dashed rectangle in Fig. 1. The model is symmetric about the center vertical and horizontal lines, with overall dimensions of AB = 100 μm and AC = 100 μm. The copper TSVs in the upper and lower Si chips are connected through a microbump of thickness (H) 20 μm and diameter (w) 20 μm. The solder thickness h is 5 μm. Outside of the microbump and between the chips, there is a possible underfill layer as depicted in Fig. 2. The influence of underfill in the bonded chip structure is specifically studied. The TSV diameter (d) is taken to be 10 μm.

Mechanical deformation is modeled through a prescribed nominal shear action under the plane strain condition. The bottom boundary AB is taken to be stationary, while the top boundary CD is under a prescribed velocity v_x of 0.5 mm/s. (When the superimposed tension or compression is considered, a v_y component is also prescribed.) The left and right boundaries are not constrained. Note that the current loading mode and boundary conditions do not give rise to a strict periodic deformation field representative of a true composite structure with repeated unit cells. However, since the main deformation action is centered around the microbump region, which is reasonably away from the

* Corresponding author.
E-mail address: shenyl@unm.edu (Y.-L. Shen).

http://dx.doi.org/10.1016/j.microrel.2016.01.004
0026-2714/

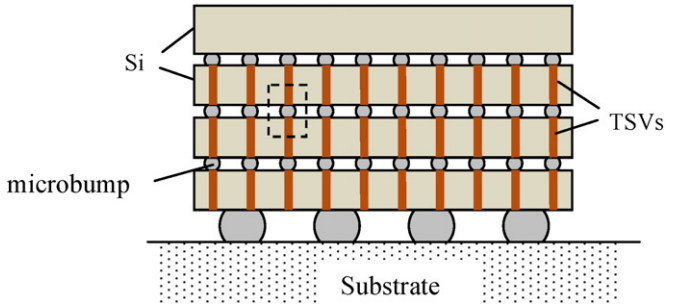

Fig. 1. Representative 3D integration scheme showing vertical stacking of Si chips containing TSVs. The schematic is not to scale, and the possible underfill material and other peripheral structures are not included.

boundaries of the model, key deformation features identical to those with periodic boundary conditions can still be obtained from the current approach [8]. In this study the nominal shear strain experienced by the solder is defined to be the prescribed horizontal displacement (v_x multiplied by time) divided by the solder height h, and the nominal tensile or compressive strains are defined in a similar way using v_y.

The finite element program Abaqus (Version 6.12, Dassault Systemes Simulia Corp., Providence, RI, USA) is employed for the computation. The model contains a total of 25,600 four-noded elements, with a finer mesh size around the microbump region. The Si and underfill material are assumed to be isotropic, linearly elastic solids. The Young's modulus and Poisson's ratio of Si are 130 GPa and 0.28, respectively; the Young's modulus and Poisson's ratio of underfill are 7.0 GPa and 0.33, respectively [9]. Copper is taken to be isotropic elastic–plastic with linear strain hardening, with its plastic yielding following the von Mises criterion and incremental flow theory. Its Young's modulus, Poisson's ratio, initial yield strength and plastic linear hardening slope are 110 GPa, 0.3, 155 MPa and 17.8 GPa, respectively [10]. The solder, taken to be the Sn–1.0Ag–0.1Cu alloy, is treated as an isotropic elastic–viscoplastic solid, with Young's modulus of 47 GPa and Poisson's ratio of 0.36. Its yielding and strain hardening response follows the experimental stress–strain curves for different strain rates [11]. At 0.005 s^{-1} strain rate or below, the initial yield strength is 20 MPa; the flow strength increases to a peak value of 36 MPa at the plastic strain of 0.15, beyond which a perfectly plastic behavior is assumed until damage is initiated (see below). This slow-rate form is

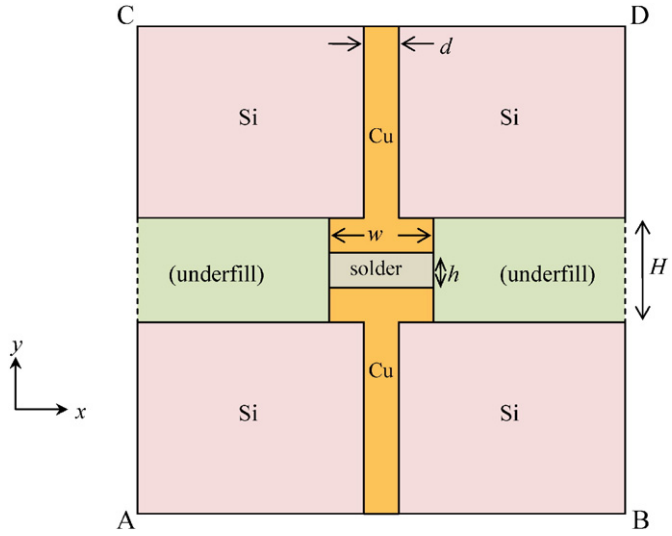

Fig. 2. Material layout used in the finite element modeling. The domain ABCD is perceived to be a representative area segment highlighted in Fig. 1.

considered as the "static" response. The rate-dependent plastic flow strength follows

$$\sigma_e = S(\bar{\varepsilon}^p)\cdot R\left(\frac{d\bar{\varepsilon}^p}{dt}\right), \tag{1}$$

where σ_e is the von Mises effective stress, S (a function of equivalent plastic strain $\bar{\varepsilon}^p$) is the static plastic stress–strain response, and R (a function of plastic strain rate $\frac{d\bar{\varepsilon}^p}{dt}$) defines the ratio of flow strength at higher strain rates to the static flow strength where R equals unity. Compared to rate-independent plasticity, this formulation utilizes the scaling parameter R to quantify the "strain rate hardening" effect. In this study the R values are 1.0, 1.9, 2.4, 2.8, 3.1, 3.4 and 3.5 at the plastic strain rates of, respectively, 0.005, 0.5, 6, 50, 100, 200 and 300 s^{-1}. It is noted that the stress–strain curves given in Ref. [11] are based on compressive tests. The present study assumes that the same rate-dependent behavior can be applied to tension, shear and multiaxial loading in general.

The simulation of solder failure utilizes a progressive ductile damage model. Fig. 3 shows a schematic of the stress–strain curve which includes the damage response (solid curve). The damage process is quantified by a scalar damage parameter D, with

$$\sigma = (1-D)\bar{\sigma}, \tag{2}$$

where σ is the current flow stress and $\bar{\sigma}$ is the flow stress in the absence of damage. In addition to leading to softening, damage is also manifested by the degradation of elastic modulus as shown by the dashed unloading/reloading line in Fig. 3. The equivalent plastic strains are $\bar{\varepsilon}_0^{pl}$ and $\bar{\varepsilon}_f^{pl}$ at the onset of damage ($D=0$) and failure ($D=1$), respectively. A material element loses its capability to carry stress when its D attains unity, at which point the element will be removed from the mesh so a "void" thus develops. Cracking is then a consequence of linking multiple adjacent voids in the model. Note that removal of an element, an evolving process throughout the simulation history determined by the computational analysis, takes place when maximum degradation is reached at any one of its integration points [12].

In general $\bar{\varepsilon}_0^{pl}$ can be made a function of the stress triaxiality, $\frac{\sigma_{hyd}}{\sigma_e}$, where $\sigma_{hyd} = \frac{1}{3}(\sigma_{xx}+\sigma_{yy}+\sigma_{zz})$ is the hydrostatic stress and σ_e is the von Mises effective stress. In the present study $\bar{\varepsilon}_0^{pl}$ is assumed to be independent of stress triaxiality due to the lack of experimental data that may be used for defining the functional form. Upon damage initiation, strain softening and thus strain localization set in, which displays a strong mesh dependency. To alleviate the problem, a characteristic length L is used in the model, with

$$\bar{u}^p = L\bar{\varepsilon}^p \tag{3}$$

where $\bar{u}^p$ represents a plastic displacement quantity, and L is defined as the square root of the integration point area in each finite element. The softening phenomenon is now expressed as a stress–displacement relationship [13]. Prior to the initiation of damage, $\bar{u}^p = 0$; after damage initiation Eq. (3) starts to take effect. Failure (and removal) of the element occurs when $\bar{u}^p$ reaches the specified failure value, $\bar{u}_f^p$. The evolution of the damage parameter is taken to follow a linear form,

$$D = \frac{\bar{u}^p}{\bar{u}_f^p}. \tag{4}$$

The damage response is thus completely specified by the two parameters $\bar{\varepsilon}_0^{pl}$ and $\bar{u}_f^p$. In the present study they are chosen to be 0.18 and 3 μm, respectively. It is noted that the chosen value of $\bar{u}_f^p$ corresponds to a $\bar{\varepsilon}_f^{pl}$ value of approximately 0.5. These parameters were